Research Letter DOI: 10.15541/jim20240493

Ablative Properties of SiC_p Doped $C_f/Li_2O\text{-}Al_2O_3\text{-}SiO_2$ Composites

LIN Yuanwei[1], JING Zhao[2], CHEN Hetuo[1], LI Jiaheng[1,4], QIN Xianpeng[1], ZHOU Guohong[1,3], WANG Shiwei[1,3]

(1. State Key Laboratory of High Performance Ceramics, Shanghai Institute of Ceramics, Chinese Academy of Sciences, Shanghai 200050, China; 2. Beijing Institute of Space Long March Vehicle, Beijing 100076, China; 3. Center of Materials Science and Optoelectronics Engineering, University of Chinese Academy of Sciences, Beijing 100049, China; 4. School of Microelectronics, Shanghai University, Shanghai 200444, China)

Abstract: In a high heat flux ablative environment, the surface temperature of aircraft rises rapidly, leading to traditional high thermal conductivity materials being ineffective at protecting internal metal components. In this study, continuous carbon fiber reinforced $Li_2O\text{-}Al_2O_3\text{-}SiO_2$ (C_f/LAS) glass ceramic composites doped with SiC particles (SiC_p) were prepared by slurry immersion winding and hot pressing sintering. Effect of matrix crystallinity on ablative properties of the composites under ultra-high heat flux was investigated. By utilizing heat absorption and low thermal conductivity characteristics associated with SiO_2 gasification within composite materials, both surface and internal temperatures of these materials are effectively reduced, thereby ensuring the safe operation of aircraft and electronic devices. Results indicate that the average linear ablation rate of composites doped with 10% (in mass) of SiC_p significantly decreases at a heat flux of 20 MW/m². Transmission electron microscope observation reveals that the doped glass matrix exhibits increased crystallinity, reduced internal stress, and minimized lattice distortion, thereby enhancing the composites' high-temperature performance. However, excessive SiC_p doping leads to reduced crystallinity and deteriorated ablation performance. Ultimately, the average linear ablation rate of C_f/LAS composites with 10% (in mass) SiC_p at 20 MW/m^2 heat flux is comparable to that of commercial carbon/carbon composites, accompanied by providing lower thermal conductivity and higher bending strength. This novel high-performance C_f/LAS composite is cost-effective, short-cycled, and suitable for mass production, offering promising potential for widespread application in ablation-resistant components of hypersonic vehicles.

Key words: ablation-resistant C_f/LAS composite; SiC doping; crystallinity of glass matrix; long-range ordered

The nozzles, leading edges and ends of spacecraft require protective materials with light weight, ultra-high temperature ablation resistance, low thermal conductivity, and excellent mechanical properties to shield the inner metallic body of spacecraft from ultra-high temperatures when re-entering the Earth's atmosphere or passing through planetary atmosphere[1-3].

Continuous carbon fiber reinforced carbon-based (C_f/C)[4-5], carbide/boride ceramic-based[6] and glass-based system composite materials[7-8] are important classes of ultra-high temperature ablation-resistant materials. Among them, C_f/C composites are extensively utilized for thermal protection, employing sublimation to absorb heat, which results in superior ablation resistance compared to materials that rely on melting for ablation[9], along with excellent high-temperature stability and mechanical strength[5, 10]. However, C_f/C composites are susceptible to oxidation[11], and require lengthy production cycles and high costs, which impede their rapid mass production[12]. Additionally, their high thermal conductivities are unfavorable for safeguarding the integrity of internal metal components[13]. Carbon fiber reinforced carbide/boride composites form oxidation-resistant films through oxidation reactions to enhance ablation resistance[14]. Nevertheless, their poor thermal shock resistance, long manufacturing cycles, high costs and high thermal conductivity limit broader applications[15-16].

Continuous carbon fiber reinforced glass-based

Received date: 2024-11-26; **Revised date:** 2025-02-19; **Published online:** 2025-02-25
Foundation item: National Natural Science Foundation of China (U23A6014, 52103357)
Biography: LIN Yuanwei (1997–), male, Master. E-mail: linyuanwei19@mails.ucas.ac.cn
林元伟(1997–), 男, 硕士. E-mail: linyuanwei19@mails.ucas.ac.cn
Corresponding author: CHEN Hetuo, associate professor. E-mail: chenhetuo@mail.sic.ac.cn;
ZHOU Guohong, professor. E-mail: sic_zhough@ mail.sic.ac.cn
陈鹤拓, 副研究员. E-mail: chenhetuo@mail.sic.ac.cn; 周国红, 研究员. E-mail: sic_zhough@mail.sic.ac.cn

ceramic material is a type of ablative material characterized by its melting properties, which utilizes a high-viscosity molten liquid film on the matrix surface at elevated temperatures to absorb external aerodynamic heat, thereby achieving heat protection[17]. This material not only exhibits excellent ablative resistance, but also offers superior heat insulation. In high heat flux ablation environments, the surface and internal temperatures of aircraft rise rapidly, posing a challenge for materials with high thermal conductivity such as C_f/C, C_f/carbide, and C_f/boride in protecting internal metal components. However, the gasification heat absorption of SiO_2 in carbon fiber reinforced glass ceramic materials can significantly reduce surface temperature. Additionally, the low thermal conductivity of glass ceramic helps maintain lower internal matrix temperature, ensuring aircraft safety and the functionality of onboard electronic devices. The production cycle of glass materials prepared through a single hot pressing process is remarkably efficient, typically only taking two weeks[18]. The low density facilitates the manufacturing of lightweight devices, while low thermal conductivity effectively prevents internal matrix failure due to overheating. Furthermore, the similar linear expansion coefficient ensures excellent compatibility with the quartz microwave windows. Compared with C_f/C, C_f/carbide and C_f/boride, the straightforward preparation process, high production efficiency, and cost-effective raw materials present promising prospects for rapid large-scale industrial production. However, traditional quartz based glass ceramic composites exhibit limitations in terms of their single performance and average ablative resistance. To address these limitations in quartz, LAS is used to modulate the matrix characteristics, yet ablation performance of LAS matrix composites with low crystallinity requires enhancement[19]. During the ablation process, the low boiling point of low-crystallinity LAS leads to excessive volatilization of SiO_2, exposing the internal carbon fiber material to the external environment. As the carbon fiber is further oxidized, it forms open pores and intensifies the ablation. To enhance the high-temperature resistance of LAS, the crystallization process can be accelerated by incorporating nucleating agents. Common nucleating agents for LAS glass include precious metal salts ($AgNO_3$), oxides (TiO_2, P_2O_5), fluorides (CaF_2, Na_3AlF_6), and carbides (SiC)[20]. SiC is particularly notable for its excellent thermal stability, and SiO_2 generated by the oxidation of SiC under high heat flow can repair the glass ceramic matrix, making it an ideal additive for LAS ablative materials.

In this study, SiC-doped C_f/LAS composites were fabricated, and their crystallization degree, ablation resistance, high-temperature thermal conductivity, and mechanical properties were explored, considering the compatibility of SiC with carbon fiber and glass matrix, as well as its anti-ablation mechanism.

1 Experimental

Sample preparation Drawing from the reported literature[18], the SiC particle-infused LAS powders were mixed with deionized water, employing carboxymethyl cellulose (CMC) as a binder and isopropyl alcohol as a dispersant, followed by ball milling utilizing agate balls. Subsequently, a continuous carbon fiber was immersed into the resulting slurry and stacked into a graphite mold after drying. The prepreg was then fabricated through hot pressing under a N_2 atmosphere of 1350 ℃ and 20 MPa. The SiC additive amounts were 0%, 10%, 20%, 30% and 40% (in mass), corresponding to C_f/LAS, C_f/LAS-SC1, C_f/LAS-SC2, C_f/LAS-SC3 and C_f/LAS-SC4, respectively. To evaluate the ablative characteristics of typical ablative materials, an identical methodology was employed to fabricate C_f/C materials.

Sample characterization The phase was analyzed by *in-situ* X-ray diffractometer (XRD, Panalytical) with a scanning rate of 6 (°)/min. Crystallinity (X) is calculated according to the following equation[21]:

$$X = \sum I_c / (\sum I_c + \sum I_a) \times 100\% \quad (1)$$

where ΣI_c is the diffraction intensity of crystalline phase, and ΣI_a is the scattering intensity of amorphous phase. The incorporation of SiC notably decreased the proportion of the amorphous phase from 62% to below 30%. The density was measured by Archimedes drainage method. The relative density (ρ_r) was calculated by comparing the measured volume density (ρ_v) to the theoretical density (ρ_t), following the mixing rule[22] $\rho_r = \rho_v / \rho_t$. Scanning electron microscope (SEM, Zeiss SUPRA 55VP) equipped with an energy dispersive spectrometer (EDS) was used to observe the micro-morphology of as-sintered composites. The three-dimensional pore distribution of the composite was obtained by three-dimensional X-ray computed tomography (X-CT, Zeiss). High-resolution lattice images of the composites were observed using a field emission transmission electron microscope (TEM, FEI Talos F200s super-X), and strain distribution was obtained by geometric phase analysis (GPA). The thermal diffusivity was measured by laser thermal conductivity meter (LFA467) by preparing a circular plate with a diameter of ~12 mm and a thickness of ~1 mm. The specific heat capacity of the sample was obtained using sapphire method and a synchronous thermal analyzer (STA449) with a controlled heating rate of 10 ℃/min. The thermal conductivity test ranged from 25 ℃ to 1000 ℃, and utilized the equation[23]:

$$\lambda = \alpha \rho C_p \tag{2}$$

where λ, α, ρ and C_p are the thermal conductivity, thermal diffusion coefficient, density and specific heat capacity at constant pressure, respectively. The sample was processed into 36 mm (length)×4 mm (width)×3 mm (thickness), and the bending strength was measured by the three-point bending method from room temperature to 1200 ℃. The bending tests of the samples were carried out on a CMT5304-30KN computer-controlled electronic universal testing machine (three-point flexural approach). The elastic moduli of the samples were determined by MHT indentation system with a diamond Berkovich indenter. The flexural strength (σ_b) and elastic modulus (E) are calculated using Eq. 3 and Eq. 4[24]:

$$\sigma_b = \frac{3PL}{2BH^2} \tag{3}$$

$$E = \frac{\Delta P L^3}{4BH^3 \Delta F} \tag{4}$$

where P, L, B, H and $\Delta P/\Delta F$ are the maximum failure load, support span, sample width, sample thickness, slope of load-displacement curve, respectively. Ablation tests were conducted using liquid oxygen-kerosene under a heat flux of 20 MW/m^2 for 10 s. For the sample exhibiting the lowest linear ablation rate, ablation tests were conducted at 30 MW/m^2 for 10 s to further explore the ablative resistance. Thickness was measured at three points before and after ablation to determine the average linear ablation rate, according to the following formula[25]:

$$R_l = \frac{d_0 - d_1}{t} \tag{5}$$

where R_l is the linear ablation rate, d_0 and d_1 are the thicknesses of the sample before and after ablation, and t is the ablation time.

2 Results and discussion

2.1 Phase composition and micro-morphology

The phase composition of C_f/LAS-SC composite is shown in Fig. 1. The C_f/LAS-SC composite primarily consists of SiC phase and LAS matrix (Fig. 1(a)). The refined XRD pattern (Fig. 1(b)) shows a χ^2 of 1.5, indicating a small fitting error. The mass percentage of crystalline SiC, crystalline LAS and other amorphous phases are obtained by the same refinement method for other samples, as depicted in Fig. 1(c). A significant rise in the relative content of crystalline LAS is observed when the SiC mass fraction is below 20%. Among them, a 10% (in mass) SiC addition yields the highest crystalline LAS content at 60%, indicating enhanced crystallization and reduced crystal defects[26]. As the SiC

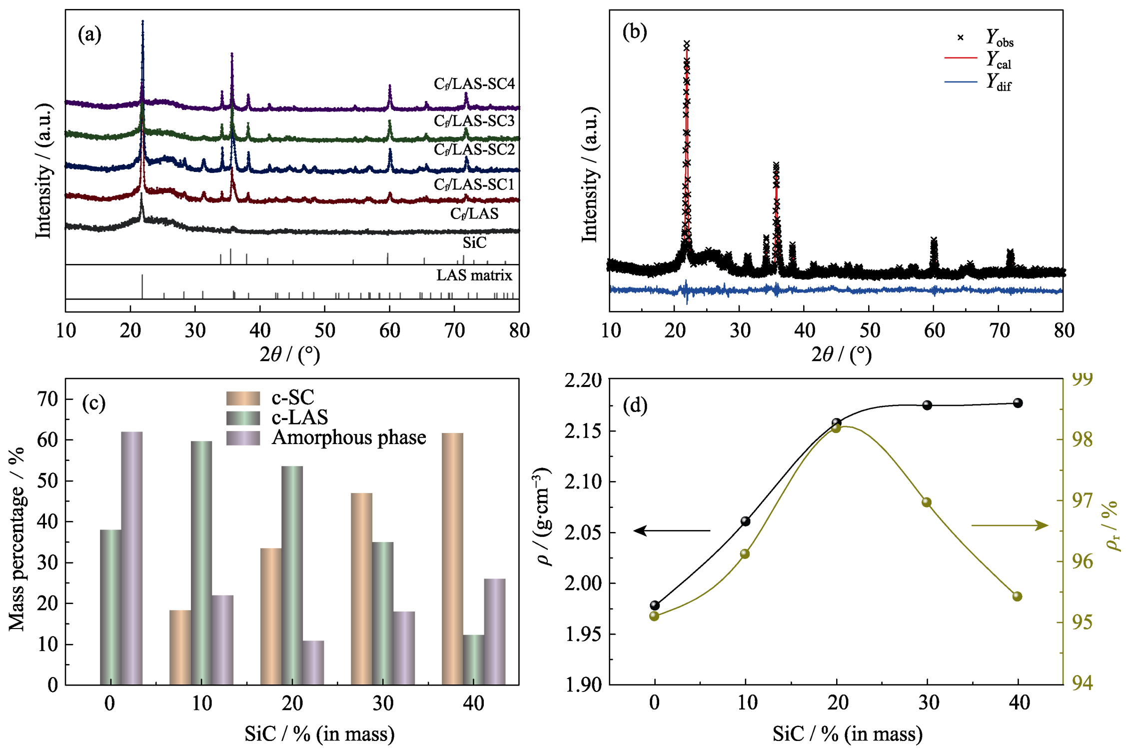

Fig. 1　Characterizations of C_f/LAS-SC composites

(a) XRD patterns; (b) XRD refined patterns of C_f/LAS-SC3; (c) Mass percentages of different phases obtained by XRD refinement (c-SC indicates crystalline SiC and c-LAS indicates crystalline LAS); (d) Density (ρ) and relative density (ρ_r)

content rises, the density of the composite material increases, with average relative density (ρ_r) in the range of 95%–99%, as depicted in Fig. 1(d). The dense LAS matrix effectively serves as an oxygen barrier at elevated temperatures, preventing direct exposure of SiC and C_f to O_2, and subsequently enhancing the material's high-temperature oxidation resistance and stability.

The cross-sectional microscopic morphology of the C_f/LAS-SC composite in Fig. 2 reveals that the LAS matrix and C_f are tightly combined. Introducing an optimal proportion of SiC_p (≤20%, Figs. 2(a-c)) results in a relatively dense LAS matrix. Conversely, an excessive addition of SiC_p (≥30%, Figs. 2(d, e)) yields a porous and loose matrix. This phenomenon is likely attributed to the high sintering temperature requirement of SiC (up to 1650 ℃[27]), where excessive SiC_p significantly elevates the densification temperature of the composite, ultimately reducing the matrix's density at lower temperatures.

Fig. 3 and Fig. 4 illustrate the microstructures of C_f/LAS and C_f/LAS-SC1 after ablation, respectively. Following the ablation process, C_f/LAS can be divided into a surface melting layer (about 200 μm thick), an intermediate transition layer (about 400 μm thick), and an internal dense layer. EDS mappings reveal that the surface melting layer and the intermediate transition layer are mainly composed of SiO_2. Due to the poor crystallinity of the C_f/LAS matrix, the carbon fibers in the transition layer fail to prevent direct oxygen exposure during high heat flux ablation, resulting in significant oxidation and the formation of a porous intermediate transition layer. Conversely, C_f/LAS-SC1 transitions from a SiO_2 melt surface layer to a dense internal layer, lacking an intermediate transition layer. These findings indicate that the highly crystalline LAS matrix effectively hinders direct contact between external oxygen and internal components, facilitating SiC oxidation to SiO_2 through O^{2-} diffusion during ablation and enhancing the composite's ablation resistance.

Fig. 5 presents TEM characterization of C_f/LAS composite material along the $[1\bar{2}1]$ zone axis. Fig. 5(a) illustrates the coexistence of crystalline and amorphous regions within the composite material. The fast Fourier transform (FFT) analysis confirms the presence of an amorphous state and a crystalline phase in LAS matrix, with diffraction rings in the amorphous region and spots in the crystalline region (Fig. 5(b)). According to the standard PDF data (39-1425), (111) and $(\bar{1}01)$ crystal plane spacings of the crystalline LAS matrix are 0.3136 and 0.4040 nm, respectively. In contrast, the (111) and $(\bar{1}01)$ crystal plane spacings of the LAS matrix in C_f/LAS are measured to be 0.2056 and 0.3169 nm, which are reduced by 34.4% and 21.6%, respectively. The narrow spacings of the (111) and $(\bar{1}01)$ crystal planes of the crystalline phase are attributed to the volume expansion of the adjacent amorphous region. The tensile stress predominantly arises in the ε_{xx} direction, while the compressive stress is primarily observed in the ε_{xy} direction. Moreover, the tensile and compressive stresses are arranged alternately along the ε_{yy} direction (Figs. 5(c-e)). High strain in amorphous region indicates a high-energy defect state, characterized by physically bonded unstable structures and excess free volume. As this excess free volume decreases, the local structure undergoes relaxation and crystallization, leading to a decrease in system energy and the formation of a stable chemically bonded structure.

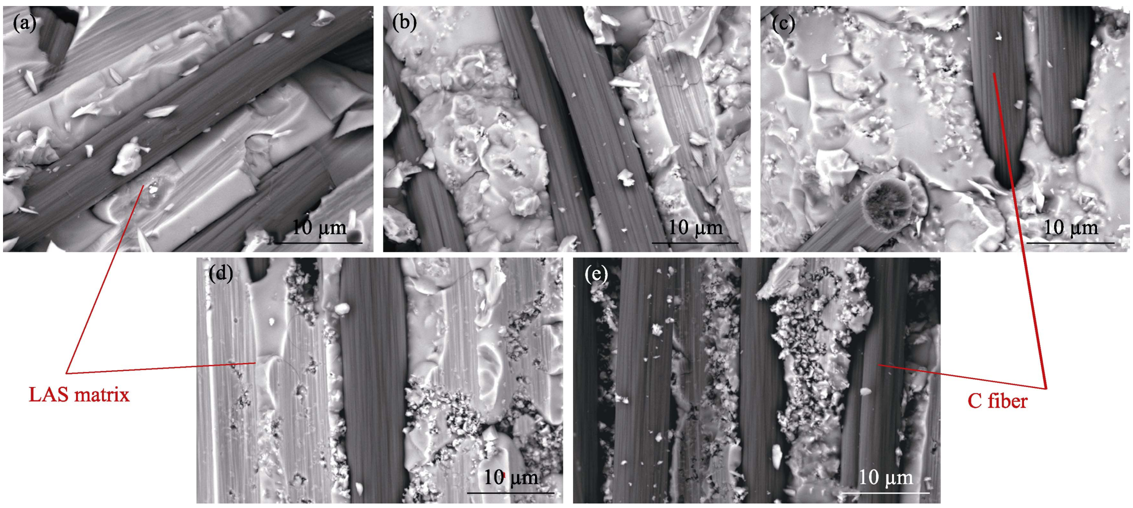

Fig. 2 Cross-sectional morphologies of C_f/LAS-SC
(a) C_f/LAS; (b) C_f/LAS-SC1; (c) C_f/LAS-SC2; (d) C_f/LAS-SC3; (e) C_f/LAS-SC4

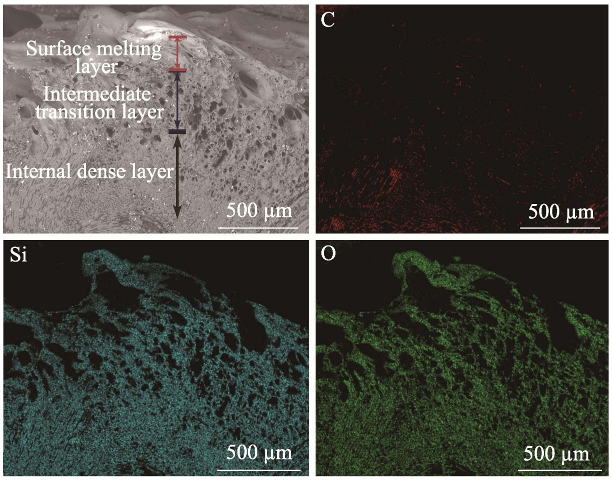

Fig. 3　Cross-sectional microscopic morphology and EDS mappings of C_f/LAS after ablation

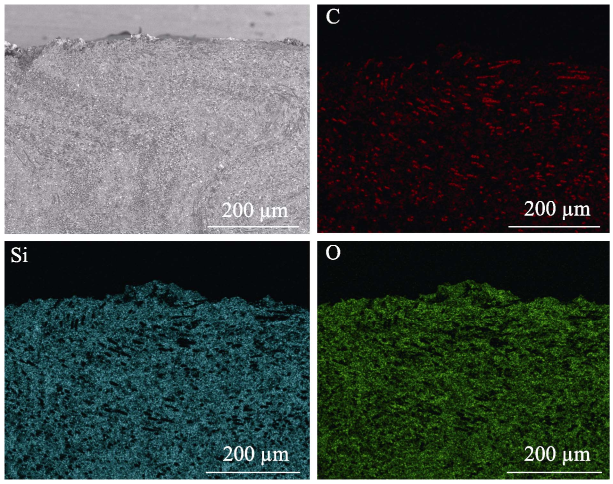

Fig. 4　Cross-sectional microscopic morphology and EDS mappings of C_f/LAS-SC1 after ablation

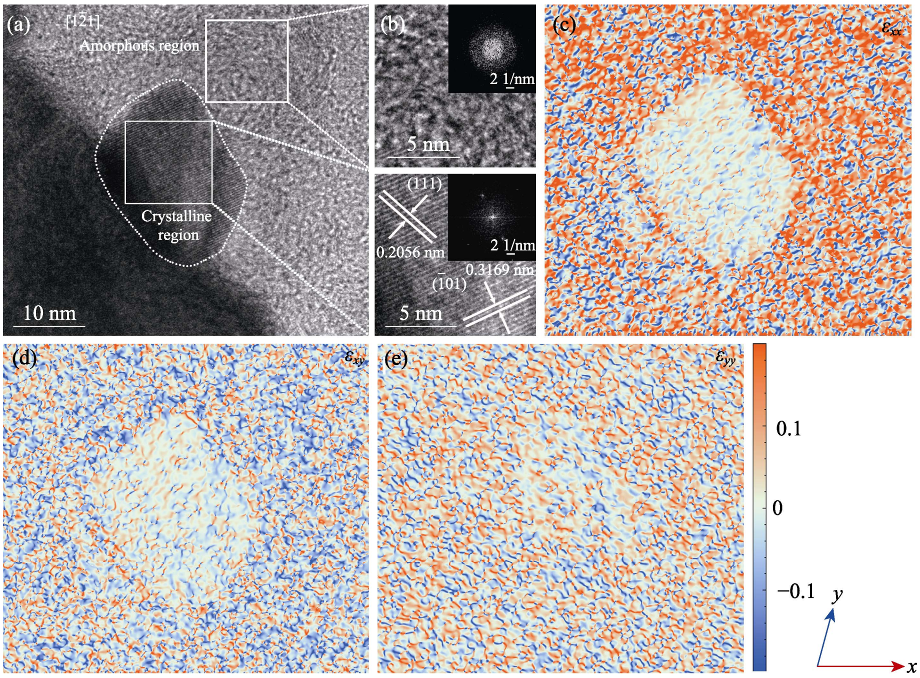

Fig. 5　TEM characterizations of C_f/LAS composite material along the $[1\bar{2}1]$ zone axis

(a) High-resolution transmission electron microscopy (HRTEM) image; (b) Images for selected regions obtained locally enlarged after the corresponding region's fast Fourier transform (FFT); (c-e) Strain distribution obtained by geometric phase analysis (GPA) of FFT

Fig. 6 presents TEM characterization of C_f/LAS-SC1 composite material along the $[1\bar{2}1]$ zone axis. In Figs. 6(a, b), the orderly atomic arrangement and diffraction spots derived from the FFT underscore its high crystallinity. Upon comparison with the standard PDF card (39-1425), the (111) crystal plane spacing of the LAS matrix in C_f/LAS-SC1 is 0.3225 nm, representing a slight increase of 2.8%, while the $(\bar{1}01)$ crystal plane spacing is 0.4100 nm, indicating a slight increase of 1.5%. Compared to C_f/LAS, the spacings of the (111) and $(\bar{1}01)$ crystal planes in C_f/LAS-SC1 align more closely with theoretical values, indicating a marked reduction in lattice distortion. The lattice primarily experiences tensile stress in the ε_{xx} direction, compressive stress in the ε_{xy} direction, and alternating stress in the ε_{yy} direction (Figs. 6(c-e)), reducing defect development and stress concentration, and bolstering the lattice's stability. The C_f/LAS-SC1 lattice exhibits lower tensile and compressive strain compared to C_f/LAS, indicating reduced internal stress (the average internal stresses of C_f/LAS and C_f/LAS-SC1 calculated by Gaussian distribution method are 110.1 and 25.3 MPa, respectively), stronger atomic bonding, and enhanced system stability.

Fig. 7 illustrates the 3D reconstructions from X-CT scans for both C_f/LAS and C_f/LAS-SC1. The reduced aperture size of C_f/LAS-SC1 corroborates SEM-EDS findings, indicating superior oxygen barrier effect properties and thus enhancing its ablative resistance.

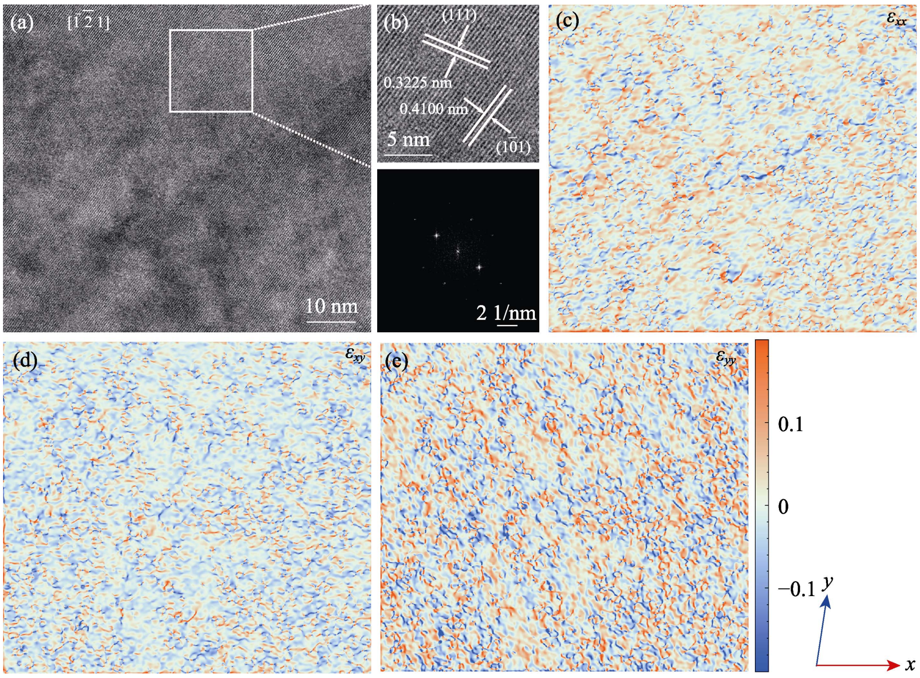

Fig. 6 TEM characterizations of C_f/LAS-SC1 composite material along the [1$\bar{2}$1] zone axis

(a) HRTEM image; (b) Images for selected regiosn obtained locally enlarged after the corresponding region's FFT; (c-e) Strain distribution obtained by GPA of FFT

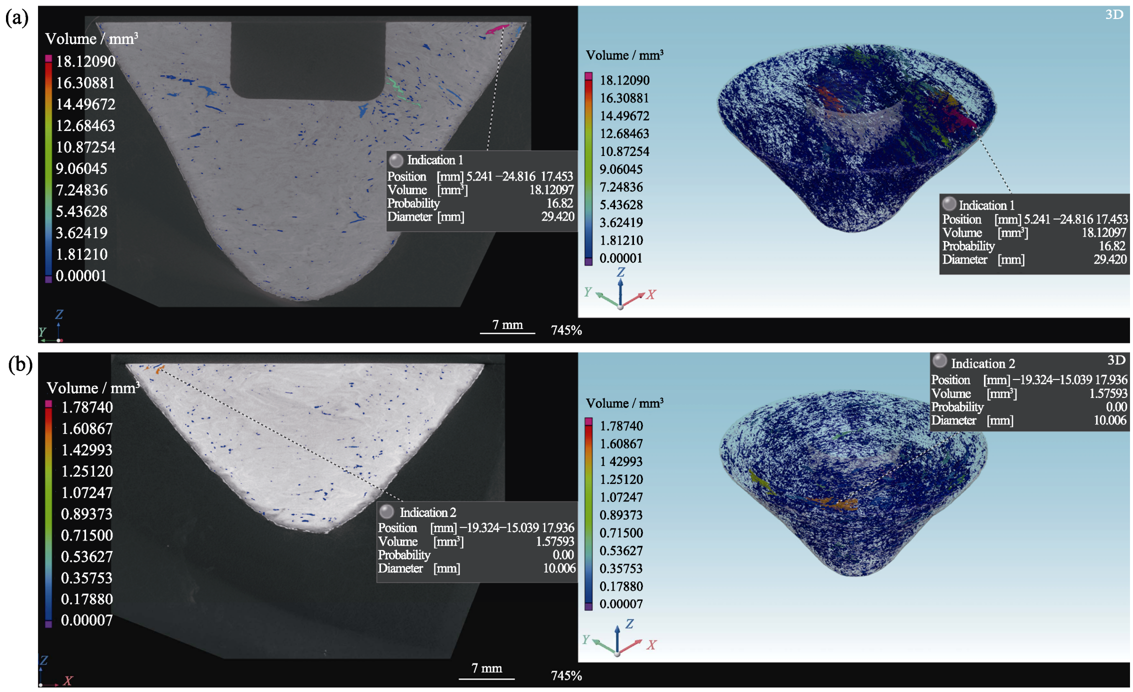

Fig. 7 X-CT 3D reconstructions of (a) C_f/LAS and (b) C_f/LAS-SC1 after ablation

2.2 Thermal performance

Fig. 8 illustrates the linear ablation rate and the underlying ablation mechanism of the sample after a 10 s ablation exposure to an ultra-high surface temperature of approximately 2400 ℃. In the high heat flux ablation environment, the volatilization of SiO_2 contributes to heat absorption within the C_f/LAS-SC, thereby reducing the surface temperature of the composite materials. At a heat flux of 20 MW/m², the surface temperature of the C_f/C composite reached 3000 ℃, while its bottom temperature reached 550 ℃. In contrast, under the same ablative conditions, the surface temperature of the C_f/LAS-SC composite is 2400 ℃, and the bottom temperature remains at ambient temperature, demonstrating superior thermal barrier properties. The introduction of an optimal amount of SiC_p effectively enhances the

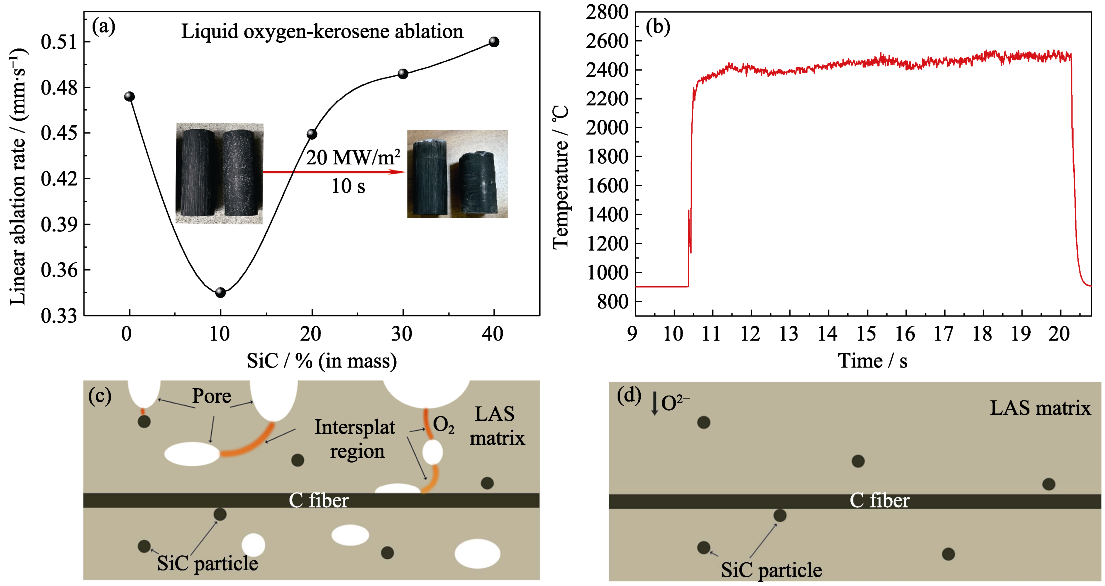

Fig. 8　(a) Average linear ablation rate with insets showing photographs of C_f/LAS-SC1 (left) and C_f/LAS (right)); (b) Surface temperature of C_f/LAS-SC; (c, d) Schematic diagrams of (c) oxygen molecule direct contact ablation and (d) oxygen ion diffusion ablation mechanism, respectively

material's ablative resistance. Specifically, at a SiC mass fraction of 10%, the linear ablation rate reaches a minimum of 0.35 mm/s under a heat flow rate of 20 MW/m^2, representing a significant reduction of ~27% (Figs. 8(a, b)). The ablative resistance of the C_f/LAS matrix is comparable to that of C_f/C, with a similar density, as indicated in Table 1[28-31]. However, an excessive SiC_p can exacerbate the ablation process.

At elevated temperatures, SiC oxidizes to form a SiO_2 repair oxide film, providing a self-healing LAS matrix that proficiently shields SiC and C_f from further oxidation. Insufficient matrix density decreases crystallinity, allowing O_2 to infiltrate the interior through pores and other imperfections (Fig. 8(c)). The high-temperature oxidation of carbon fibers and excess SiC (>10%) produces CO and CO_2 gases, resulting in a foam liquid layer that fails to effectively prevent ablation, thereby deteriorating the ablative properties. The oxidation reactions of the composite material are described by the following chemical equations:

$$2SiC(s)+3O_2(g)\rightarrow 2SiO_2(s)+2CO(g) \quad (6)$$

$$SiC(s)+2O_2(g)\rightarrow SiO_2(s)+CO_2(g) \quad (7)$$

$$C(s)+O_2(g)\rightarrow CO_2(g) \quad (8)$$

The C_f/LAS-SC glass-ceramic matrix with a high level of crystallization, offers superior O_2 barrier properties, and undergoes ablation behavior driven by O^{2-} diffusion (Fig. 8(d)). Under simulated ablative conditions of liquid oxygen kerosene, the LAS matrix has sufficient density, allowing both the dense matrix and the SiO_2 layer to effectively prevent direct contact between O_2 and the interior. The high-temperature oxidation of SiC forming a SiO_2 film facilitates the internal diffusion of O^{2-}, and the corresponding chemical reaction equations are given as:

$$SiC+4O^{2-}\rightarrow SiO_2+CO_2+8e^- \quad (9)$$

$$O_2+4e^-\rightarrow 2O^{2-} \quad (10)$$

An appropriate addition of SiC can rectify defects caused by CO_2 and inherent lattice imperfections by producing SiO_2. This process enhances the densification of the SiO_2 layer and significantly mitigates the ablation rate.

Fig. 9 depicts the thermal conductivity curve of the C_f/LAS-SC1 at different temperatures. During the aircraft's re-entry into Earth's atmosphere, considerable aerodynamic heating generates a significant heat flux across the surface layer of the C_f/LAS-SC. Notably, low thermal conductivity of the C_f/LAS system's materials minimizes the risk of overheating in the inner layers, thus averting potential safety hazards.

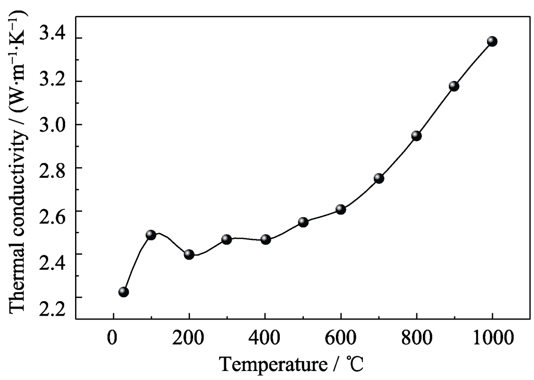

Fig. 9　Thermal conductivity of C_f/LAS-SC1

As the temperature rises, the material's crystallinity enhances, subsequently enhancing its thermal conductivity[32]. This direct relationship between temperature and thermal conductivity protects the sample from local overheating, deformation, or cracking resulting from thermal stress concentration during the heating process. Additionally, within the tested temperature range, the thermal conductivity of the C_f/LAS matrix remains below 3.5 W/(m·K), substantially lower than that of C_f/C, effectively preventing the internal metal material from overheating failures or posing safety hazards (Table 1)[28-31].

2.3 Mechanical properties

Fig. 10 exhibits the mechanical properties of C_f/LAS-SC. Within the tested temperature range, the bending strength of all specimens remains above 125 MPa, demonstrating remarkable mechanical stability even after prolonged high-temperature exposure. Specifically, C_f/LAS exhibits superior bending strength at lower temperatures, while SiC-doped samples perform better at elevated temperatures (Fig. 10(a)).

From a thermodynamic standpoint, the internal energy of C_f/LAS-SC glass-ceramics exceeds that of their crystalline state, resulting in a thermodynamically unstable yet metastable condition. As temperatures surpass 1000 ℃, heightened molecular vibrations facilitate crystallization through rearrangement and orientation[33-34]. This process reduces porosity within the glass structure, enhancing its interlocking characteristics. Consequently, the bending strength and elastic modulus of C_f/LAS-SC glass-ceramics reach optimal values around 1000 ℃ (Figs. 10(a, c)).

Notably, C_f/LAS-SC3 achieves a remarkable bending strength of 407.3 MPa at 1100 ℃. However, this performance is accompanied by excessive maximum displacement and deformation. As depicted in Fig. 10(b), higher temperatures increase the maximum displacement of the samples, which helps to distribute internal stress and improves high-temperature stability. For instance, C_f/LAS-SC2 exhibited a relatively small maximum displacement below 1000 ℃, resulting in stress concentration and deformation at higher temperatures, similar to other samples. In contrast, C_f/LAS-SC1 exhibits a large maximum displacement at low temperatures, effectively relieving internal stress and preventing deformation at elevated temperatures.

Table 1 Properties of C_f/C and C_f/LAS ablative composites[29-31]

Composition	ρ/(g·cm^{-3})	λ/(W·m^{-1}·K^{-1})	Ablation at high heat flux: Ablation rate/(mm·s^{-1})	Test environments	Ablation time/s	Ref.
C_f/C	1.85	45–68 (25–800 ℃)	–	Oxyacetylene torch with a heat flux of 3.9 MW/m^2	60	[28]
	1.80	–	1.2–1.4	Stagnation ablation by high temperature air ionization jet	3	[29]
		–	0.114	Nitrogen plasma jet with a heat flux of ~25 MW/m^2	20	[30]
	1.80	–	0.699	Stagnation ablation by air plasma flame with a heat flux of 22.1 MW/m^2	3	[31]
	–	–	0.245	Liquid oxygen-kerosene, and the heat flux at 30 MW/m^2	10	This work
C_f/LAS-SiC1	2.03	2.2–3.4 (25–1000 ℃)	0.35	Liquid oxygen-kerosene, and the heat flux at 20 MW/m^2	10	This work
			0.70	Liquid oxygen-kerosene, and the heat flux at 30 MW/m^2	10	

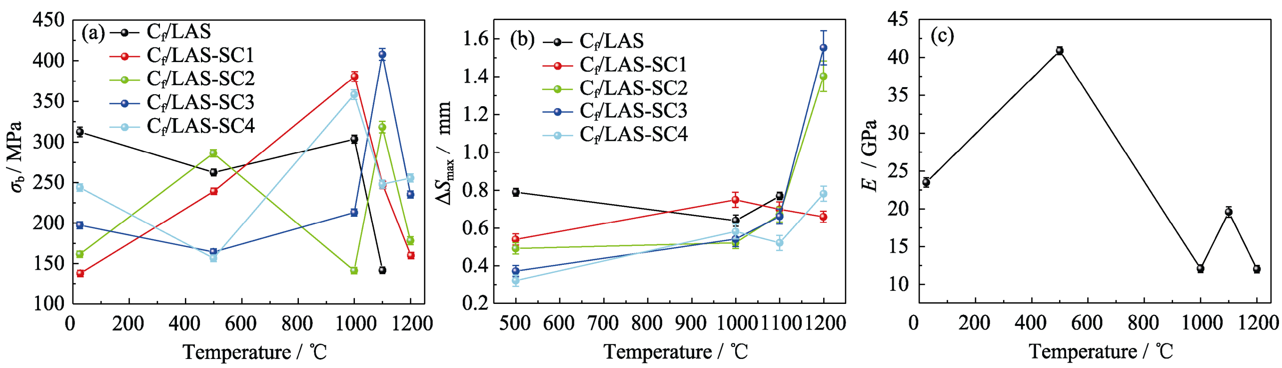

Fig. 10 Mechanical properties of C_f/LAS-SC

(a) Curves of temperature-bending strength relationship; (b) Curves of temperature-maximum displacement relationship; (c) Curve of temperature-elastic modulus relationship for C_f/LAS-SC1

3 Conclusions

In the extreme high heat flux ablation environment, the internal and external temperatures of the aircraft sharply rise, making conventional high thermal conductivity materials inadequate for protecting internal metal components. This study investigates the influences of crystallinity on the ablation resistance of carbon fiber-reinforced glass ceramic matrix composites, known for their low thermal conductivity. Integrating 10% (in mass) SiC_p into the C_f/LAS glass-ceramic matrix composite enhances its crystallinity. The diffusion of O^{2-} ions during the oxidation reduces the average linear ablation rate by ~27%. SiC efficiently repairs the antioxidant film, preventing direct exposure of the internal structure to the ablative environment. Simultaneously, the crystallization transition relieves internal stress, reduces lattice distortion and defect concentration, and enhances system's stability and compactness, thereby improving ablation resistance. However, excessive addition of SiC_p lowers the density of the C_f/LAS glass composite and elevates its amorphous phase. The CO_2 produced by SiC undermines the anti-oxidation film, exacerbating material ablation. The crystallization of the C_f/LAS glass reduces voids, strengthening its mechanical properties at elevated temperatures. Consequently, 10% (in mass) SiC-reinforced C_f/LAS glass composites exhibit compelling properties of ablation resistance, low thermal conductivity, and high-temperature strength, making them suitable candidates for hypersonic vehicles.

References:

[1] YE Z M, ZENG Y, XIONG X, *et al*. Elucidating the role of preferential oxidation during ablation: insights on the design and optimization of multicomponent ultra-high temperature ceramics. *Journal of Advanced Ceramics*, 2022, **11(12):** 1956.

[2] LYU Y, HAN Z H, ZHAO G D, *et al*. Efficient fabrication of light C_f/SiHfBOC composites with excellent thermal shock resistance and ultra-high-temperature ablation up to 1800 ℃. *Journal of Advanced Ceramics*, 2023, **12(11):** 2062.

[3] FAN Q G, CUI H, YAN L S, *et al*. Ablation resistance properties of ultra-high temperature composites C/C-SiC-ZrB_2 by slurry impregnation method. *Journal of Inorganic Materials*, 2013, **28(9):** 1014.

[4] KUMAR C V, KANDASUBRAMANIAN B. Advances in ablative composites of carbon based materials: a review. *Industrial & Engineering Chemistry Research*, 2019, **58(51):** 22663.

[5] XU L, LI X C, NI L Y, *et al*. Ablation behavior of functional gradient ceramic coating for porous carbon-bonded carbon fiber composites. *Corrosion Science*, 2018, **142:** 145.

[6] XU X T, PAN X H, NIU Y R, *et al*. Difference evaluation on ablation behaviors of ZrC-based and ZrB_2-based UHTCs coatings. *Corrosion Science*, 2021, **180:** 109181.

[7] SUI H, ZHANG H, GAO L F, *et al*. Boron and nitrogen doping in fused silica ceramics: structural, high-temperature mechanical and long-term ablation resistance properties of Si-B-O-N ceramics. *Silicon*, 2024, **16(12):** 5147.

[8] QUINTAL C C, CORMONT P, GALLAIS L. Experimental and numerical investigation of CO_2 laser ablation of fused silica with sub-microsecond pulses. *Journal of Applied Physics*, 2021, **130(9):** 093106.

[9] FARHAN S, WANG R M, LI K Z, *et al*. Sublimation and oxidation zone ablation behavior of carbon/carbon composites. *Ceramics International*, 2015, **41(10):** 13751.

[10] ZHANG W Z, TAN M Y, CHEN D M, *et al*. Sugar-derived nanocrystalline graphite matrix C/C composites with excellent ablative resistance at 3000 ℃. *Advanced Materials*, 2024, **36(7):** 2309899.

[11] CHENG L F, XU Y D, ZHANG L T, *et al*. Oxidation behavior of carbon-carbon composites with a three-layer coating from room temperature to 1700 ℃. *Carbon*, 1999, **37(6):** 977.

[12] FERREIRA J R, COPPINI N L, NETO F L. Characteristics of carbon-carbon composite turning. *Journal of Materials Processing Technology*, 2001, **109(1/2):** 65.

[13] HAN X, ZHANG S Y, LI W, *et al*. Preparation and thermal conductivity of C/C composites filled with diamond particles. *Diamond and Related Materials*, 2018, **88:** 85.

[14] WANG P P, LI H J, JIA Y J, *et al*. Ablation resistance of HfB_2-SiC coating prepared by *in-situ* reaction method for SiC coated C/C composites. *Ceramics International*, 2017, **43(15):** 12005.

[15] ZHAO J J, CAI R, MA Z K, *et al*. Preparation and properties of C/SiC composites reinforced by high thermal conductivity graphite films. *Diamond and Related Materials*, 2021, **116:** 108376.

[16] HE Z J, LI C, YANG B, *et al*. Interfacial reaction and brazing behaviour of SiC_f/SiC with C_f/C composites using Si-10Zr alloy at high temperatures. *Journal of the European Ceramic Society*, 2021, **41(2):** 1142.

[17] ZOU C R, LI B, MENG X J, *et al*. Ablation behavior and mechanism of SiO_{2f}/SiO_2, SiO_{2f}/BN and Si_3N_{4f}/BN radar wave transparent composites. *Corrosion Science*, 2018, **139:** 243.

[18] ZHOU G H, WANG S W, HUANG X X, *et al*. Unidirectional carbon fiber and SiC particulate co-reinforced fused silica composite. *Ceramics International*, 2007, **33(7):** 1395.

[19] VENKATESWARAN C, SREEMOOLANADHAN H, VAISH R. Lithium aluminosilicate (LAS) glass-ceramics: a review of recent progress. *International Materials Reviews*, 2022, **67(6):** 620.

[20] CHEN F, XU X R, XIA W W, *et al*. Practical nucleator agents for lithium aluminum silicate glass-ceramics. *Glass*, 2023, **50(11):** 32.

[21] ZHANG Y Y, ZHANG X M, GUO L X, *et al*. Effect of temperature-dependent nano SiC on the ablation resistance of ZrC coating. *Journal of the European Ceramic Society*, 2024, **44(12):** 6875.

[22] SCHERER, G. W. Sintering of low-density glasses: I, theory. *Journal of the American Ceramic Society*, 1977, **60(5/6):** 236.

[23] YANG X, SU X L, YAN Y G, *et al*. Structures and thermoelectric properties of $(GeTe)_nBi_2Te_3$. *Journal of Inorganic Materials*, 2021, **36(1):** 75.

[24] LI T, ZHANG Y L, ZHANG J, *et al*. Improved antioxidative and mechanical properties of SiC coated C/C composites *via* a SiO_2-SiC reticulated layer. *Journal of the European Ceramic Society*, 2021, **41(13):** 6151.

[25] XIE W Q, ZHANG B, GE B Z, *et al*. Exceptionally low ablation rates realized in the cellular-structured MCMB@WC composites *via* biomimetic design. *Composites Part A: Applied Science and Manufacturing*, 2024, **179:** 108035.

[26] YUAN X B, LI R, XIONG Z, *et al*. Synergistic crystallization modulation and defects passivation *via* additive engineering stabilize perovskite films for efficient solar cells. *Advanced Functional Materials*, 2023, **33(24):** 2215096.

[27] DING Y S, DONG S M, HUANG Z R, *et al*. Fabrication of short C fiber-reinforced SiC composites by spark plasma sintering. *Ceramics International*, 2007, **33(1):** 101.

[28] ZAMAN W, LI K Z, IKRAM S, *et al*. Residual compressive and thermophysical properties of 4D carbon/carbon composites after repeated ablation under oxyacetylene flame of 3000 ℃. *Transactions of Nonferrous Metals Society of China*, 2013, **23(6):** 1661.

[29] YIN J, XIONG X, ZHANG H B, *et al*. Microstructure and ablation performances of dual-matrix carbon/carbon composites. *Carbon*, 2006, **44(9):** 1690.

[30] SHEN X T, SHI Z Q, ZHAO Z G, *et al*. Study of the ablation of a carbon/carbon composite at ~25 MW/m^2 with a nitrogen plasma torch. *Journal of the European Ceramic Society*, 2020, **40(15):** 5085.

[31] YIN J, ZHANG H B, XIONG X, *et al*. Ablation properties of C/C-SiC composites tested on an arc heater. *Solid State Sciences*, 2011, **13(11):** 2055.

[32] ZHOU W X, CHENG Y, CHEN K Q, *et al*. Thermal conductivity of amorphous materials. *Advanced Functional Materials*, 2020, **30(8):** 1903829.

[33] TAKAMORI T, ROY R. Rapid crystallization of SiO_2-Al_2O_3 glasses. *Journal of the American Ceramic Society*, 1973, **56(12):** 639.

[34] SKORODUMOVA O B, SEMCHENKO G D, GONCHARENKO Y N, *et al*. Crystallization of SiO_2 from ethylsilicate-based gels. *Glass and ceramics*, 2001, **58:** 31.

SiC_p掺杂C_f/Li_2O-Al_2O_3-SiO_2复合材料耐烧蚀性能研究

林元伟[1], 景 昭[2], 陈鹤拓[1], 李佳恒[1,4], 覃显鹏[1], 周国红[1,3], 王士维[1,3]

(1. 中国科学院 上海硅酸盐研究所, 关键陶瓷材料全国重点实验室, 上海 200050; 2. 北京航天长征飞行器研究所, 北京 100076; 3. 中国科学院大学 材料与光电研究中心, 北京 100049; 4. 上海大学 微电子学院, 上海 200444)

摘 要: 在高热流密度烧蚀环境中, 飞行器的表面温度迅速升高, 导致传统高导热材料无法有效保护内部金属部件。本研究通过浆液浸渍缠绕和热压烧结法制备了 SiC 颗粒(SiC_p)掺杂的连续碳纤维增强低导热 Li_2O-Al_2O_3-SiO_2 (C_f/LAS)玻璃陶瓷复合材料, 研究了基体结晶度对超高热流密度下复合材料烧蚀性能的影响规律。利用复合材料中 SiO_2 气化吸热和低导热的特性, 有效降低了复合材料表面和内部温度, 从而保障了飞行器和电子器件的安全运行。结果显示, 在 20 MW/m^2 热流密度下, 10%(质量分数)SiC_p 掺杂的复合材料平均线性烧蚀率显著降低。透射电镜结果表明, 掺杂后的玻璃基体结晶度提高, 内应力降低, 晶格畸变减少, 从而增强了复合材料的高温性能。然而, 当 SiC 掺杂量过高时, 结晶度降低, 烧蚀性能变差。最终, 在 30 MW/m^2 热流密度下, 10%(质量分数)SiC_p 掺杂的 C_f/LAS 复合材料的平均线性烧蚀率与商用碳/碳复合材料相当, 且具有较低的导热性和较高的抗弯强度。这种新型高性能 C_f/LAS 复合材料价格低廉、周期短, 适合大规模生产, 有望广泛应用于高超音速飞行器耐烧蚀部件。

关 键 词: 耐烧蚀 C_f/LAS 复合材料; SiC 掺杂; 玻璃基体结晶度; 长程有序

中图分类号: TB35 **文献标志码:** A **文章编号:** 1000-324X(2025)10-1153-10